Research in Astronomy and Astrophysics, 22:115015 (15pp), 2022 November https://doi.org/10.1088/1674-4527/ac93d4

HT Lyn and IR Lyn: Two Semi-detached-type Near-contact Binaries with Stable Orbital Period

Zi-Bin Meng[1], Hong-Wei Wang[1], Yun-Xia Yu[1,2], Ke Hu[1,2], and Fu-Yuan Xiang[1,2]
[1] Key Laboratory of Star and Interstellar Medium, Xiangtan University, Xiangtan 411105, China; yu.sunny@126.com
[2] Department of Physics, Xiangtan University, Xiangtan 411105, China
Received 2022 May 25; revised 2022 September 19; accepted 2022 September 20; published 2022 November 2

Abstract

We presented the first photometric and orbital period investigations for two near-contact binaries: HT Lyn and IR Lyn. The light-curves solutions derived from both our ground-based and various surveys' observations suggested that HT Lyn and IR Lyn are two semi-detached-type near-contact binaries with the secondary and primary components filling the Roche lobe. Combining the eclipse timings derived from several surveys' data and our observations with those reported in the literature, we modified the orbital periods and revealed that their orbital periods were stable for the last two decades. The absolute physical parameters were well determined by using the empirical relations and the Gaia-distance-based method. Similar to other near-contact binaries, the primary components of HT Lyn and IR Lyn are evolving at the main-sequence stage, while their less-massive secondary components show the over-sized and over-luminosity features and should be more evolved than their primary ones. Combining the stable orbital period with the semi-detached configurations, we infer that the two near-contact binaries may be just located in the critical phase and evolving from the current semi-detached phase to the detached or contact one.

Key words: (stars:) binaries (including multiple): close – (stars:) binaries: eclipsing – stars: evolution – stars: individual (HT Lyn, IR Lyn)

Online material: machine-readable tables

1. Introduction

Near-Contact Binary (NCB) is a special subtype of close binaries defined by Shaw et al. (1990). They are not in contact like the W UMa-type binaries, but the facing surfaces of their two components are very close to each other (less than 0.1 orbital radius apart, Shaw 1994). According to the prediction of thermal relaxation oscillation (TRO) theory (Flannery 1976; Lucy 1976; Robertson & Eggleton 1977), the detached binary must undergo a few dozen TROs around the marginal contact state to achieve the over-contact phase. Therefore, they are unique sources for testing the TRO theory. Besides, NCBs may be the best samples for exploring the physical process of mass transfer frequently occurring in semi-detached and contact binaries. In theory, the continuous mass transfer could yield impacting spot on the surface of the acceptor component (Shaw et al. 1990; Pavlovski et al. 1998; Qian & Zhu 2002; Zhu et al. 2010; Hu et al. 2019). Because the spectral type of the cooler component of an NCB is later about one or two spectral types than its hotter component, its two components have, in general, a relatively large temperature difference. Moreover, unlike over-contact binaries, the NCBs have not yet built a thick common convective envelope. These observational facts make the impacting spot to be photometrically observed more easily than that in the over-contact binaries. However, from the observational side, the NCBs are relatively rare because their evolutionary time is very short relative to the lifetime of close binary (Zhu & Qian 2006; Zhu et al. 2010; Zejda et al. 2016). The accumulated samples for NCBs are not yet enough to establish reliable statistics for testing these theoretical predictions (Zhu et al. 2010).

In this paper, we present the first multi-band photometric observations for two NCBs: HT Lyn (=GSC 02968-00253) and IR Lyn (=BD+52 1270=TYC 3414-2292-1). They were discovered by the Northern Sky Variability Survey (NSVS,[3] Woźniak et al. 2004). Subsequently, they were observed by the Wide Angle Search for Planets (WASP,[4] Butters et al. 2010) and the Catalina Sky Survey (CSS) telescope used by the Catalina Real-Time Transient Survey (CRTS,[5] Drake et al. 2009). According to the photometric observations of the two surveys, HT Lyn and IR Lyn are classified as variables with EB-type light curves (Khruslov 2013). At the same time, Khruslov (2013) determined the preliminary elements, such as the orbital period and the amplitudes of their light curves, etc.

[3] http://skydot.lanl.gov/nsvs/nsvs.php
[4] https://wasp.cerit-sc.cz/form
[5] http://crts.caltech.edu/

Table 1
Parameters of Target, Comparison, and Check Stars

Object	α_{2000}	δ_{2000}	B (mag)	V (mag)	Period	Parallax (mas)
HT Lyn	$07^h54^m19\overset{s}{.}508$	$43°02'11\overset{''}{.}423$	13.823	13.567	0.564396	0.577(27)
AP6349378	$07^h54^m14\overset{s}{.}670$	$43°01'16\overset{''}{.}902$	14.348	13.358	⋯	0.530(24)
AP6349386	$07^h54^m23\overset{s}{.}621$	$43°03'44\overset{''}{.}159$	15.444	14.156	⋯	0.466(23)
IR Lyn	$08^h02^m30\overset{s}{.}461$	$51°54'10\overset{''}{.}986$	10.331	9.947	0.513304	4.498(39)
TYC 3414-2415-1	$08^h03^m22\overset{s}{.}854$	$51°56'14\overset{''}{.}583$	12.438	11.672	⋯	3.228(41)
TYC 3414-2170-1	$08^h01^m54\overset{s}{.}945$	$51°55'08\overset{''}{.}514$	11.151	10.593	⋯	3.758(32)

Recently, five surveys, i.e., the Zwicky Transient Facility (ZTF,[6] Bellm et al. 2019; Masci et al. 2019), the Kamogata-KisoKyoto Wide-field Survey (KWS),[7] the All-Sky Automated Survey for SuperNovae (ASAS-SN,[8] Shappee et al. 2014; Jayasinghe et al. 2019), the Gaia mission[9] (Gaia Collaboration et al. 2016, 2018), and the Transiting Exoplanet Survey Satellite (TESS,[10] Ricker et al. 2015) also scanned the two targets. Although these surveys' observations covered a wide time interval, they were either discontinuous, or significantly low-precision, or in a wide/single band. For instance, both KWS and ASAS-SN have discontinuously observed the two targets for more than five years, but their observational data show a rather large scatter due to the very low precision. TESS has continuously monitored the two targets with relatively high precision for two elliptical orbit periods (27.4 days[11]). However, these observations have been performed with a long cadence (30 minutes) and a wide band (approximately 600–1000 nm). For the spectroscopic observation, HT Lyn and IR Lyn were scanned by the Large Sky Area Multi-Object Fiber Spectroscopic Telescope (LAMOST,[12] Luo et al. 2015) spectral survey, and the spectroscopic elements about them were revealed. Although many photometric and spectroscopic observations from various surveys have been performed, a detailed investigation involving the photometric nature and evolutionary status of the two systems is missing.

2. Observations and Data Reduction

The multi-band photometric observations for the two binaries: HT Lyn and IR Lyn, were made with the 85 cm reflecting telescope at the Xinglong Station of the National Astronomical Observatories, Chinese Academy of Sciences. The telescope was equipped with Cassegrain-focus multi-color Charge-Coupled Device (CCD) photometer, which has 2048×2048 square pixels. During our observations, Johnson-cousins BVR filters and an Andor DZ936 PI2048 CCD photometric system were mounted. HT Lyn was observed on 2017 February 10 and 12. The exposure time for each image was 70 s, 60 s and 50 s for B, V, and R bands, respectively. IR Lyn was observed on 2018 January 21 and 23. Because it is a relatively bright source, the exposure time was set as 12 s for B filter, 6 s for V filter and 4 s for R filter. From those observations, we obtained a total of 819 images (273 in B band, 274 in V band, and 272 in R band) for HT Lyn, and 3004 images (1004 in B band, 1002 in V band, and 998 in R band) for IR Lyn, respectively. All observed CCD images were processed using the Image Reduction and Aperture Photometry packages in the `Image Reduction and Analysis Facility` (`IRAF`[13]) in standard fashion. In their respective fields of view, two stars that are as close to the corresponding targets as possible, were selected as the comparison and check stars, respectively. Because the comparison star we chose was close enough to the target and the air-mass difference between the target and comparison stars was very small. Therefore, an extinction correction for the data was not made. From the Set of Identifications, Measurements and Bibliography for Astronomical Data (SIMBAD) database, we collected their basic information, e.g., the orbital periods, coordinates, V-band magnitudes, and parallax, which is listed in Table 1. The photometric data for HT Lyn and IR Lyn are presented as the magnitude differences between the target and comparison stars in Tables 2 and 3, respectively. The phases are calculated based on the orbital periods determined by Khruslov (2013). The corresponding phase-folded light curves are depicted in Figure 1. As seen in the lower panel of Figure 1, the different magnitudes between the comparison and check stars are flat, thus indicating that the brightness of the comparison star is constant throughout the observations. The light curves of both HT Lyn and IR Lyn show the typical EB-type luminosity variations, implying that they should be in contact or near-contact geometrical configuration. The luminosity of the primary eclipse is significantly lower than those of the secondary eclipse, suggesting that the temperatures of their

[6] https://www.ztf.caltech.edu/
[7] http://kws.cetus-net.org/maehara/VSdata.py
[8] https://asas-sn.osu.edu/
[9] https://www.cosmos.esa.int/gaia
[10] https://tess.mit.edu
[11] TESS is a space-based telescope launched in 2018 April and placed in a highly elliptical orbit with a period of 13.7 days.
[12] http://www.lamost.org/public/
[13] `IRAF` is distributed by the National Optical Astronomy Observatory (NOAO), which is operated by the Association of the Universities for Research in Astronomy, Inc., under cooperative agreement with the National Science Foundation (NSF). http://iraf.noao.edu/.

Table 2
BVR Bands Photometric Data of HT Lyn

B Band			*V* Band			*R* Band		
HJD	Phase	Δm	HJD	Phase	Δm	HJD	Phase	Δm
2457794.96316	0.8433	−0.536	2457794.96644	0.8491	−0.001	2457794.96681	0.8498	0.365
2457794.96590	0.8482	−0.534	2457794.96789	0.8517	0.005	2457794.96826	0.8523	0.350
2457794.96735	0.8507	−0.525	2457794.96977	0.8550	0.010	2457794.97029	0.8560	0.366
2457794.96906	0.8538	−0.527	2457794.97240	0.8597	0.022	2457794.97292	0.8606	0.374
2457794.97169	0.8584	−0.533	2457794.97438	0.8632	0.025	2457794.97490	0.8641	0.365
2457794.97366	0.8619	−0.521	2457794.97635	0.8667	0.043	2457794.97686	0.8676	0.385
2457794.97563	0.8654	−0.504	2457794.97833	0.8702	0.040	2457794.97884	0.8711	0.396
2457794.97761	0.8689	−0.510	2457794.98029	0.8737	0.037	2457794.98081	0.8746	0.387
…	…	…	…	…	…	…	…	…
2457797.20347	0.8127	−0.582	2457797.20217	0.8104	−0.031	2457797.20650	0.8181	0.329
2457797.20543	0.8162	−0.568	2457797.20409	0.8138	−0.035	2457797.20824	0.8211	0.328
2457797.20717	0.8193	−0.580	2457797.20609	0.8173	−0.021	2457797.21073	0.8256	0.329
2457797.20960	0.8236	−0.574	2457797.20785	0.8205	−0.021	2457797.21256	0.8288	0.334
2457797.21143	0.8268	−0.559	2457797.21028	0.8248	−0.013	2457797.21440	0.8321	0.342
2457797.21326	0.8300	−0.559	2457797.21212	0.8280	−0.014	2457797.21692	0.8365	0.347
2457797.21582	0.8346	−0.545	2457797.21395	0.8313	−0.014			
			2457797.21650	0.8358	−0.005			

Note. The full data set of Table 2 is compiled as a supplementary file (mst1-mrt.txt) in machine-readable format. Here a portion is presented for guidance regarding its form and content.

(This table is available in its entirety in machine-readable form.)

primary components eclipsed on phase 0.0 are significantly higher than those of the secondary components.

3. Orbital Period Investigations

With the photometric data of two surveys: NSVS and WASP, Khruslov (2013) derived the linear ephemerides of HT Lyn and IR Lyn as

$$\text{Min.I} = \text{HJD2454800.938} + 0.564396E, \quad (1)$$

and

$$\text{Min.I} = \text{HJD2454504.394} + 0.513304E, \quad (2)$$

respectively. Because the photometric observations for the two early surveys are in a wide band and their accuracies are very low, the linear ephemerides of HT Lyn and IR Lyn, perhaps, are not very reliable. In order to determine the exact ephemeris and uncover possible period variations, we perform a careful search for all available eclipse timings of the two binary systems. However, there exists only one eclipse timing for HT Lyn and IR Lyn, respectively. Thus, from the databases of all available surveys, we extracted the photometric data for the two targets, aiming to derive some eclipse timings and determine their optimal photometric solutions. In view of the relatively continuous observations of WASP and ZTF in *r* band, we derived the eclipse timings directly from these photometric data by using the Kwee–van Woerden (K-W) method (Kwee & van Woerden 1956). For the discontinuous photometric observations from NSVS, KWS, and ASAS-SN, we first calculated the phase-folded light curves according to the observational seasons, and then calculated the eclipse timings with the method of Borkovits et al. (2015). For the long-cadence observations from TESS, we applied the algorithm proposed by Wang (2017) and Li et al. (2020, 2021) to determine the eclipse timings. In addition, from our observations, we calculated two eclipse timings for HT Lyn and IR Lyn, respectively. Finally, a total of 46 data points for HT Lyn and 40 data points for IR Lyn were obtained and compiled in Table 4. With Equations (1) and (2), we calculated the $O-C$ values for those eclipse timings of HT Lyn and IR Lyn, and constructed the $O-C$ diagrams (see Figure 2). From Figure 2, any significant nonlinear variations could not be found from the $O-C$ curves of both HT Lyn and IR Lyn, implying their orbital period should be stable at least in the last 20 yr. With the least-squares method, we revised the linear ephemerides of HT Lyn and IR Lyn as

$$\text{Min.I} = \text{HJD2454800.9376(7)} + 0.5643942(2)E, \quad (3)$$

and

$$\text{Min.I} = \text{HJD2454504.3948(9)} + 0.5133074(2)E, \quad (4)$$

respectively. The corresponding residuals are shown in the bottom panel of Figure 2.

4. Light-curves Solutions

We analyzed the *BVR* light curves of HT Lyn and IR Lyn, using the 2015 version of the `Wilson-Devinney` (`W-D`) code (Wilson & Devinney 1971; Wilson 1979, 1990;

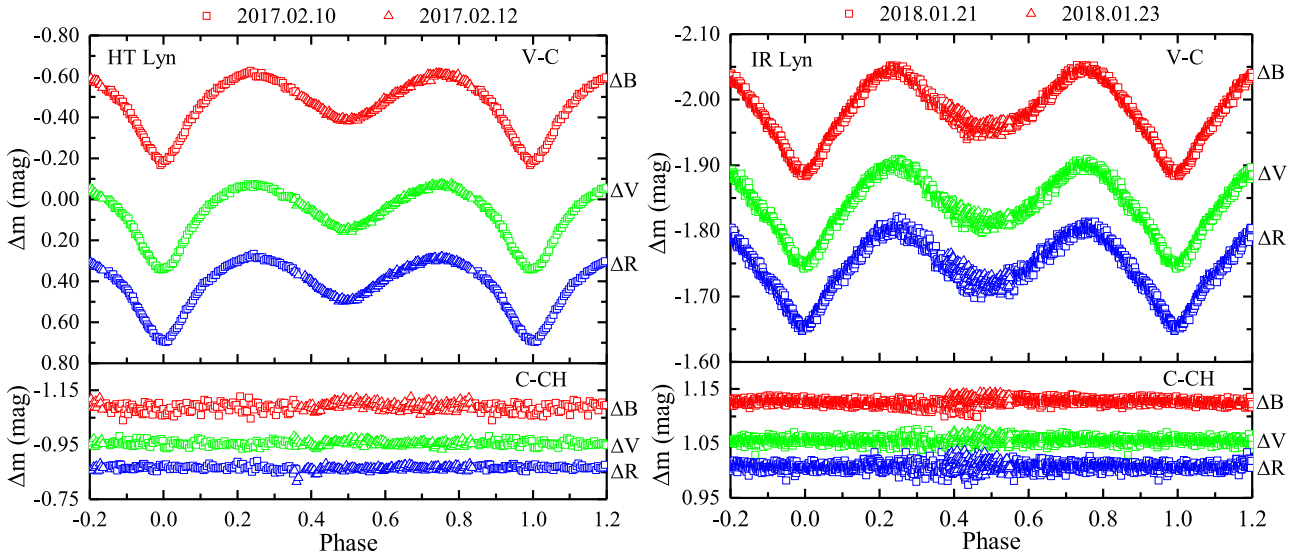

Figure 1. The observed light curves for HT Lyn (left panel) and IR Lyn (right panel). The corresponding magnitude differences between the comparison and check stars are shown in their bottom panels.

Table 3
BVR Bands Photometric Data of IR Lyn

B Band			*V* Band			*R* Band		
HJD	Phase	Δm	HJD	Phase	Δm	HJD	Phase	Δm
2458141.96902	0.5413	−1.963	2458141.96957	0.5424	−1.818	2458141.96927	0.5419	−1.731
2458141.96945	0.5422	−1.959	2458141.97000	0.5432	−1.818	2458141.96969	0.5426	−1.718
2458141.96987	0.5430	−1.955	2458141.97043	0.5440	−1.820	2458141.97011	0.5434	−1.742
2458141.97029	0.5438	−1.957	2458141.97114	0.5454	−1.810	2458141.97054	0.5442	−1.734
2458141.97098	0.5452	−1.953	2458141.97163	0.5463	−1.820	2458141.97126	0.5457	−1.710
2458141.97147	0.5461	−1.964	2458141.97212	0.5473	−1.818	2458141.97175	0.5467	−1.715
2458141.97295	0.5471	−1.966	2458141.97308	0.5493	−1.820	2458141.97222	0.5475	−1.735
2458141.97243	0.5479	−1.965	2458141.97355	0.5502	−1.824	2458141.97271	0.5485	−1.743
…	…	…	…	…	…	…	…	…
2458144.02325	0.5434	−1.963	2458144.02468	0.5461	−1.827	2458144.02662	0.5498	−1.734
2458144.02412	0.5449	−1.969	2458144.02512	0.5469	−1.807	2458144.02707	0.5508	−1.728
2458144.02456	0.5459	−1.963	2458144.02561	0.5479	−1.815			
2458144.02499	0.5467	−1.966	2458144.02606	0.5488	−1.819			
2458144.02547	0.5477	−1.956	2458144.02650	0.5496	−1.809			
2458144.02592	0.5484	−1.967	2458144.02695	0.5504	−1.820			
2458144.02637	0.5494	−1.958						
2458144.02681	0.5502	−1.967						

Note. The full data set of Table 3 is compiled as a supplementary file (mst2-mrt.txt) in machine-readable format. Here a portion is presented for guidance regarding its form and content.

(This table is available in its entirety in machine-readable form.)

Wilson & Van Hamme 2014). First, we determine the preliminary temperatures of two binary systems: HT Lyn and IR Lyn, according to two color indices: $J-H$ (Two Micron All Sky Survey, Skrutskie et al. 2006) and $g-i$ (Sloan Digital Sky Survey, Alam et al. 2015), as well as the temperatures estimated from the distance-independent colors $G_{BP}-G$ and $G-G_{RP}$ of the Gaia (Andrae et al. 2018) and the spectroscopic observations from LAMOST. In Table 5, the temperatures corresponding to the $J-H$ and $g-i$ dereddened color indices, are estimated by using the corrected calibration of Pecaut & Mamajek (2013) and the flux calibrated spectral type standards of Covey & Ivezić (2007), respectively. The interstellar

Table 4
Eclipse Timings of HT Lyn and IR Lyn Collected from Literature and Calculated from Our Observations and Surveys' Data

HT Lyn				IR Lyn			
HJD	Error	Type	References	HJD	Error	Type	References
2451464.80554	0.00421	p	(1)	2451574.18523	0.01127	s	(1)
2451465.08284	0.00513	s	(1)	2451574.44574	0.00737	p	(1)
2454066.65763	0.00042	p	(2)	2454418.66870	0.00215	p	(2)
2454068.63720	0.00125	s	(2)	2454436.63800	0.00140	p	(2)
2454083.59180	0.00152	p	(2)	2454437.66930	0.00094	p	(2)
2454084.72480	0.00078	p	(2)	2454438.68933	0.00178	p	(2)
2454085.55220	0.00282	s	(2)	2454501.56442	0.00169	s	(2)
2454092.61756	0.00136	p	(2)	2454504.39400	⋯	p	(3)
2454094.61390	0.00104	s	(2)	2454524.41347	0.00069	p	(2)
2454099.67917	0.00241	s	(2)	2454526.49162	0.00099	p	(2)
2454101.65389	0.00077	p	(2)	2454527.48599	0.00148	p	(2)
2454111.52820	0.00122	s	(2)	2454534.41706	0.00213	s	(2)
2454120.56416	0.00093	s	(2)	2454544.43006	0.00136	p	(2)
2454122.53360	0.00107	p	(2)	2454547.51011	0.0009	p	(2)
2454141.44060	0.00087	s	(2)	2456667.47796	0.00462	p	(8)
2454146.52444	0.00062	s	(2)	2456667.72697	0.00523	s	(8)
2454150.47300	0.00082	s	(2)	2457053.47444	0.00388	p	(8)
2454156.39559	0.00034	p	(2)	2457053.74006	0.00656	s	(8)
2454163.45037	0.00060	s	(2)	2457398.93869	0.00399	p	(8)
2454165.42674	0.00036	p	(2)	2457399.18774	0.00672	s	(8)
2454167.40920	0.00063	s	(2)	2457761.84557	0.0036	p	(8)
2454170.50830	0.00044	p	(2)	2457762.09231	0.00961	s	(8)
2454438.60317	0.00040	p	(2)	2458125.77500	0.00308	p	(8)
2454533.42052	0.00031	p	(2)	2458126.03871	0.00653	s	(8)
2454800.93800	⋯	p	(3)	2458142.20456	0.00056	p	(5)
2456877.34304	0.00221	p	(4)	2458144.00031	0.00100	s	(5)
2456877.62467	0.00234	s	(4)	2458493.30044	0.00585	p	(8)
2457393.47967	0.00274	s	(4)	2458493.57381	0.00979	s	(8)
2457393.76285	0.00106	p	(4)	2458845.69246	0.00018	s	(7)
2457795.05156	0.00047	p	(5)	2458845.94832	0.00006	p	(7)
2457797.02680	0.00071	s	(5)	2458851.59465	0.00009	p	(7)
2457902.57017	0.00412	s	(4)	2458851.85204	0.00019	s	(7)
2457902.84582	0.00172	p	(4)	2458859.55178	0.00014	s	(7)
2458503.92780	0.00119	p	(6)	2458859.80773	0.00003	p	(7)
2458511.83035	0.00046	p	(6)	2458861.34824	0.00346	p	(8)
2458845.66829	0.00074	s	(7)	2458861.60123	0.00571	s	(8)
2458845.95117	0.00064	p	(7)	2458865.45383	0.00007	p	(7)
2458846.79945	0.00410	s	(6)	2458865.71147	0.00019	s	(7)
2458849.90125	0.00068	p	(6)	2459217.58623	0.00308	p	(8)
2458851.59440	0.00042	p	(7)	2459217.84769	0.01041	s	(8)
2458851.87645	0.00057	s	(7)				
2458853.85086	0.00031	p	(6)				
2458860.34258	0.00049	s	(7)				
2458860.62545	0.00068	p	(7)				
2458865.42187	0.00051	s	(7)				
2458865.70455	0.00075	p	(7)				

References. (1) This paper (NSVS); (2) This paper (WASP); (3) Khruslov (2013); (4) This paper (ASAS-SN); (5) This paper (our observations); (6) This paper (ZTF); (7) This paper (TESS); (8) This paper (KWS).

extinction for different filters was derived using the S&F method (Schlafly & Finkbeiner 2011) from the IRAS database.[14] The last column of Table 5 presents the averaged values of those temperatures determined from different methods, and the corresponding errors represent the standard deviations. However, for HT Lyn, we did not adopt the temperature corresponding to the LAMOST spectrum to calculate the average temperature because the low-resolution

[14] https://irsa.ipac.caltech.edu/applications/DUST/

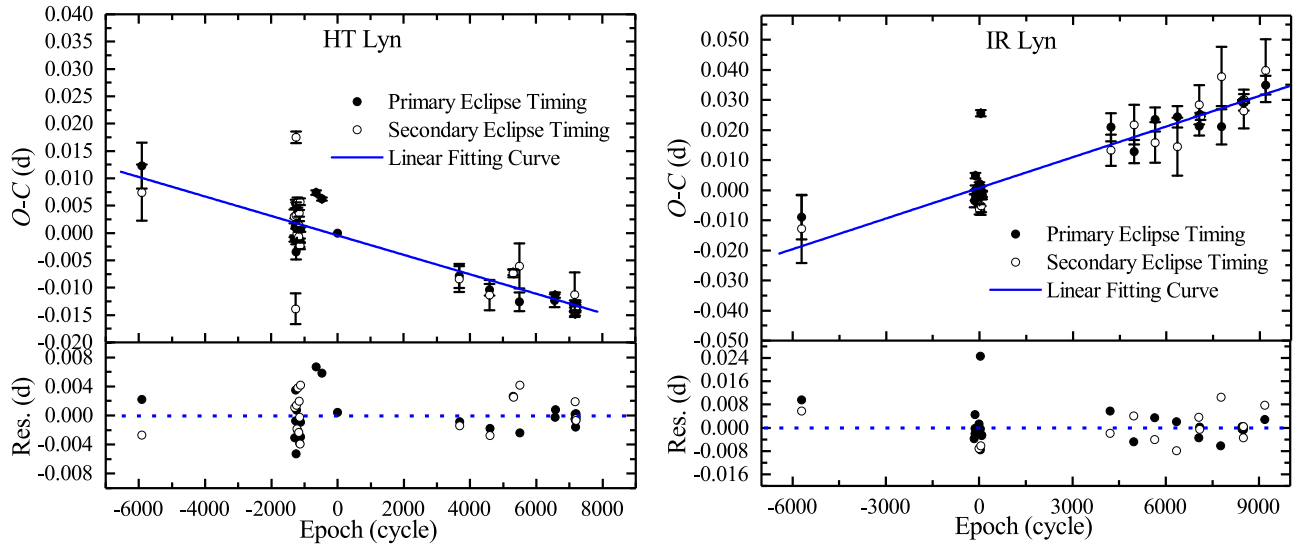

Figure 2. $O-C$ diagrams for HT Lyn (left) and IR Lyn (right). The open and filled circles refer to the primary and secondary eclipse timings, respectively. The solid lines are the linear fitting curves. The corresponding residuals are plotted in the lower panel.

Table 5
Temperature of HT Lyn and IR Lyn

Target	$T_{\rm JH}$	$T_{\rm gi}$	$T_{\rm G}$	$T_{\rm L}$	$T_{\rm est}$
HT Lyn	7440	7569	7820	A2V	7610(158)
IR Lyn	6412	6867	6746	6745(F5V)	6693(170)

spectrum of HT Lyn provided by LAMOST is significantly deviated from the spectral profile of a normal star, resulting that the temperature cannot be determined and only an approximate spectral type of A2V was roughly estimated by LAMOST. Moreover, the temperature of 8840 K estimated from the approximate spectral type is significantly deviated from those determined by those color indices. The average temperatures are not the temperature for any one of two components, but the quadrature temperature of their two components. Thus, the average temperatures are only adopted as the preliminary ones ($T_{\rm pre}$) of the primary components. During the light-curves analysis, the final temperatures of the primary and secondary components would be further adjusted according to the following equation (Kjurkchieva & Vasileva 2015)

$$T_1^f = T_{\rm pre} + \frac{c\Delta T}{c+1}, \qquad T_2^f = T_1^f - \Delta T, \tag{5}$$

where c is the ratio of the relative luminosity of two components calculated by applying the standard weighted average method to three bands, and $\Delta T = T_{\rm pre} - T_2$.

Additionally, we needed to determine the gravity-darkening and the bolometric albedos coefficients for the two systems. As has been pointed out by Kaluzny (1985), the photometric solutions for close binaries are very sensitive to the choice of the gravity-darkening coefficient. Usually, the gravity-darkening and bolometric albedos coefficient could be assumed as 1.00 for stars with the radiative envelope, and be set to 0.32 and 0.50 for stars with the convective envelope (Lucy 1967; Ruciński 1969). Empirically, the threshold temperature from the radiative to the convective envelope is generally assumed to be about 7200 K (Zhu & Qian 2006). Because the estimated temperature is higher than 7200 K for HT Lyn, and significantly lower than 7200 K for IR Lyn, the gravity-darkening coefficients of the components are set to $g_1 = 1.0$ and $g_2 = 0.32$ for HT Lyn, and $g_1 = g_2 = 0.32$ for IR Lyn (Lucy 1967). The bolometric albedos coefficients are set to $A_1 = 1.0$ and $A_2 = 0.5$ for HT Lyn, and $A_1 = A_2 = 0.5$ for IR Lyn (Ruciński 1969). Finally, the limb-darkening law with the square-root function was adopted and the corresponding coefficients were taken from the table of van Hamme (1993). When the temperatures of the components are modified according to Equation (5), the limb-darkening coefficients would also be adjusted.

Due to the absence of photometric and spectroscopic mass ratios for both HT Lyn and IR Lyn, we need to estimate a suitable mass ratio as the initial one. Here, we applied the customary q-search method to search for the initial mass ratio. In view of the sufficient data points of IR Lyn, the observations in each band were binned into 100 normal points by the standard weighted average calculation. The weighted uncertainty for each normal point was taken as the corresponding error and used to calculate the weights of the normal points according to the formula $w_i = 1/\sigma_i^2$. The typical EB-type light curves of HT Lyn and IR Lyn indicate that their geometrical configurations could be any one of the following four models: Detached model (D), Contact model (C), Semi-Detached model with primary filling Roche lobe (SD1), and Semi-Detached model with the secondary filling its Roche lobe (SD2). In the

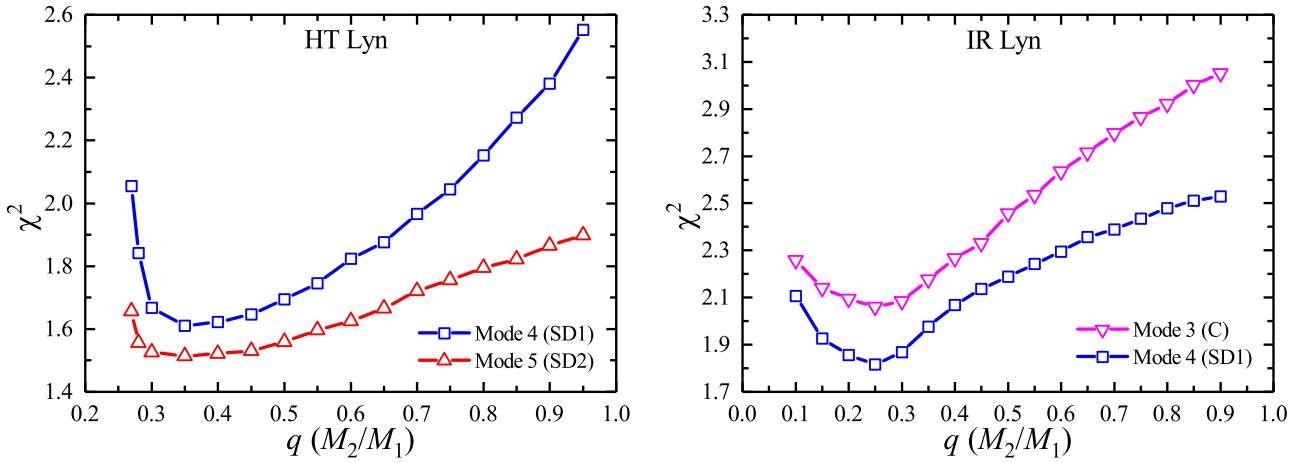

Figure 3. Relations between chi-square χ^2 and mass ratio q.

W-D code, they are denoted as modes 2, 3, 4, and 5, respectively. For each mode, we have performed many trial runs for several distinct mass ratios. It is found that the photometric solution of HT Lyn can converge for only modes 4 and 5, while for IR Lyn, it could converge for modes 3 and 4. Moreover, they can well converge only when the mass ratios are lower than 1.0, implying that their primary stars have a more massive mass than the secondary stars. In addition, the temperatures of the secondary stars for both HT Lyn and IR Lyn are significantly lower than 7200 K, confirming that both the gravity-darkening and bolometric albedos coefficients for the secondary are set reasonably. A detailed search for the mass ratio q ranging from 0.25 to 1.00 was then performed for those converging models of HT Lyn and IR Lyn. Figure 3 displays the relations between the chi-square ($\chi^2 = \frac{1}{\nu}\sum_{i=1}^{n}\frac{(O_i - C_i)^2}{\sigma_i^2}$, where n and σ_i denote the total number of data points and the errors, respectively, and ν denotes the number of degrees of freedom of the data set) and the mass ratio ($q = M_2/M_1$). For HT Lyn, a minimal value of χ^2 occurs at $q = 0.35$, while for IR Lyn, χ^2 achieves the minimal value at $q = 0.25$. These mass ratios were adopted as the initial free parameters to separately carry out various models. The other adjustable parameters are the orbital inclination i, the effective temperature of the secondary star T_2, the dimensionless potentials of two components Ω_1 and Ω_2, and the monochromatic luminosity of the primary component in the different bands, i.e., L_{1B}, L_{1V}, and L_{1R}. The relative luminosity of the secondary star was calculated with the blackbody radiation model.

Based on the above initial settings, we run the W-D code until the best converging solutions are obtained. Then, the effective temperatures of components around the preliminary value $T_{\rm pre}$ are further modified according to Equation (5). Also, the bolometric and monochromatic coefficients of the limb-darkening law are adjusted by interpolating from the table of van Hamme (1993). After many iterations, we obtained the final and self-consistent solutions for those different models, which are shown in Table 6. The theoretical light curves and the corresponding residuals are displayed in Figure 4. Apparently, the theoretical light curves for the different models can fit the observational data satisfactorily. However, for HT Lyn, the chi-square value χ^2 for the SD2 is somewhat smaller than that of SD1, while for IR Lyn, the chi-square value of SD1 is significantly smaller than that of SD2. These suggest that HT

Table 6
Photometric Solutions of HT Lyn and IR Lyn

Target Name	HT Lyn		IR Lyn	
Model	Mode4 (SD1)	Mode5 (SD2)	Mode3 (C)	Mode4 (SD1)
i(degree)	72.16(35)	69.76(13)	52.80(31)	56.70(16)
g_1, g_2	1.00,0.32	1.00,0.32	0.32,0.32	0.32,0.32
A_1, A_2	1.00,0.50	1.00,0.50	0.50,0.50	0.50,0.50
$\Omega_{\rm in}$	2.629	2.589	2.301	2.388
Ω_1	2.629	2.593(10)	2.294(8)	2.388
Ω_2	2.827(20)	2.589	2.294(8)	2.766(16)
T_1(K)	7729	7768	6762	6720
T_2(K)	5243(20)	5296(19)	4539(60)	4216(128)
$q = \frac{M_2}{M_1}$	0.376(6)	0.357(4)	0.228(3)	0.265(10)
$\frac{L_1}{L_1+L_2}$ (B)	0.9706(27)	0.9827(29)	0.9949(22)	0.9943(27)
$\frac{L_1}{L_1+L_2}$ (V)	0.9507(32)	0.9686(30)	0.9892(31)	0.9882(36)
$\frac{L_1}{L_1+L_2}$ (R)	0.9311(36)	0.9521(32)	0.9812(37)	0.9795(42)
r_1 (pole)	0.4377(14)	0.4412(12)	0.4789(13)	0.4657(18)
r_1 (side)	0.4678(17)	0.4718(16)	0.5192(17)	0.5022(22)
r_1 (back)	0.4942(16)	0.4977(17)	0.5431(18)	0.5266(25)
r_2 (pole)	0.2437(48)	0.2740(8)	0.2436(47)	0.1872(22)
r_2 (side)	0.2504(54)	0.2855(9)	0.2537(56)	0.1902(23)
r_2 (back)	0.2668(72)	0.3182(9)	0.2877(102)	0.1976(28)
$f = \frac{\Omega_{\rm in}-\Omega}{\Omega_{\rm in}-\Omega_{\rm out}}$	...	...	4.8(5.5)%	...
χ^2	1.591	1.508	2.047	1.766

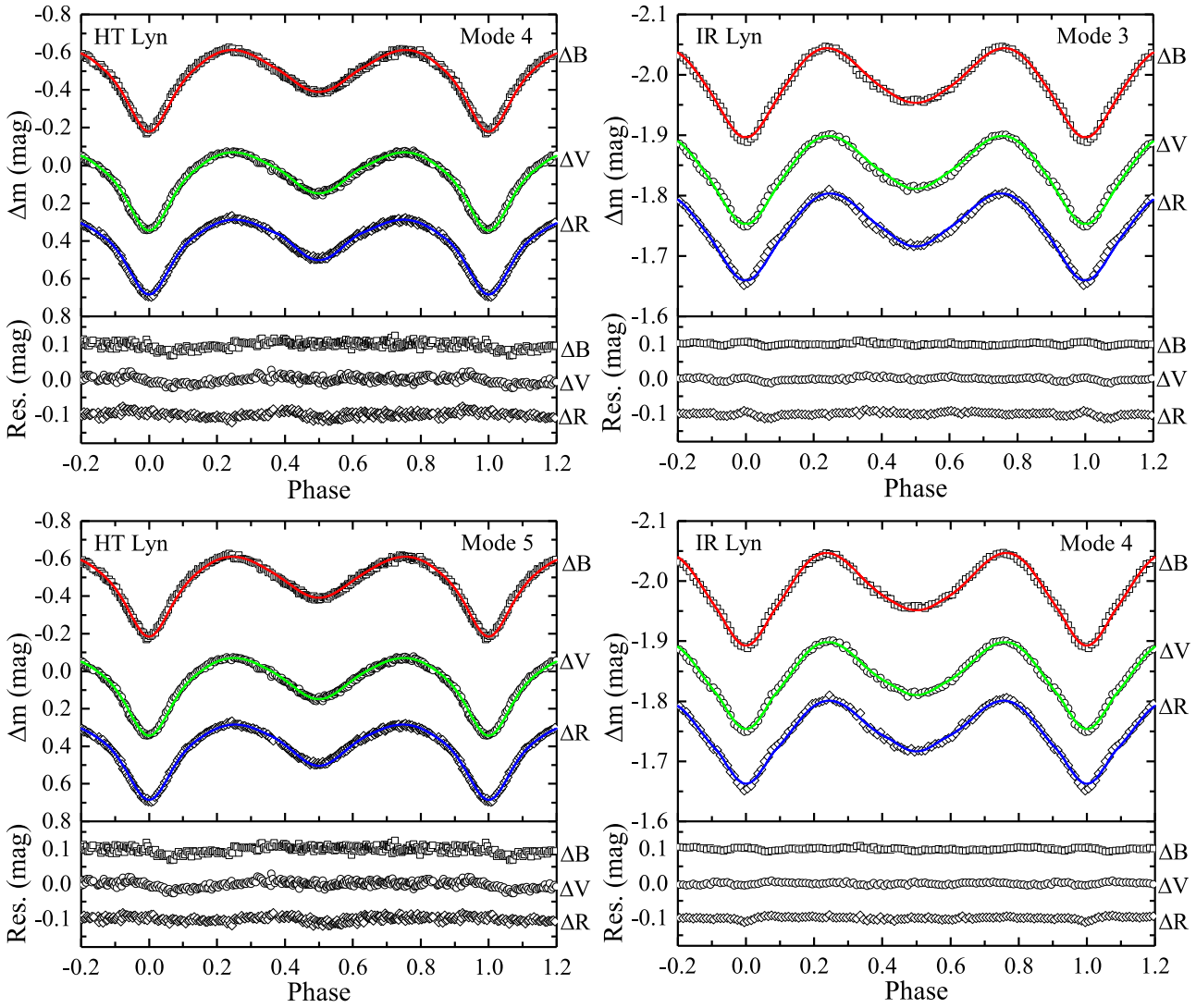

Figure 4. Observed (open symbols) and theoretical (solid lines) light curves of HT Lyn (left) and IR Lyn (right). The theoretical light curves are calculated according to the photometric solutions listed in Table 6.

Lyn tends toward the semi-detached model with the secondary filling Roche lobe, while IR Lyn tends toward the semi-detached model with the primary filling Roche lobe. In order to check the photometric solutions and determine the models for HT Lyn and IR Lyn more firmly, we also applied the W−D code to analyze those photometric data from various surveys. Among those surveys, the data product of TESS includes the Single Aperture Photometry (SAP) and the Pre-search Data Conditioning (PDC) light curves. The latter has been processed to make it more suitable for detecting shallow transits of extrasolar planets, and not intended for eclipse binaries which show large variability amplitudes. Thus, we adopted only the SAP data in the present work. The SAP flux data are downloaded from Mikulski Archive for Space Telescopes (MAST), and we excluded the data points with a nonzero flag for the QUALITY parameter. In view of the SAP flux data errors are not provided in the MIT Quick Look Pipeline (QLP) light curve files on MAST (Huang et al. 2020), we adopted the residual sum of squares as the goodness-of-fit criterion for the TESS light curves. The observed light curves from various surveys and the theoretical light curves are shown in Figure 5. The final photometric solutions are summarized in Tables 7 and 8. Clearly, these converging solutions for various surveys' light curves do not significantly deviate from those derived from our multi-band light curves. By comparing the chi-square values, we may infer that HT Lyn and IR Lyn should be the semi-detached binary with the secondary and primary filling Roche lobe, respectively. Thus, in the following analyses, we would adopt the photometric solutions of modes 5 (SD2) and 4 (SD1) for HT Lyn and IR Lyn, respectively.

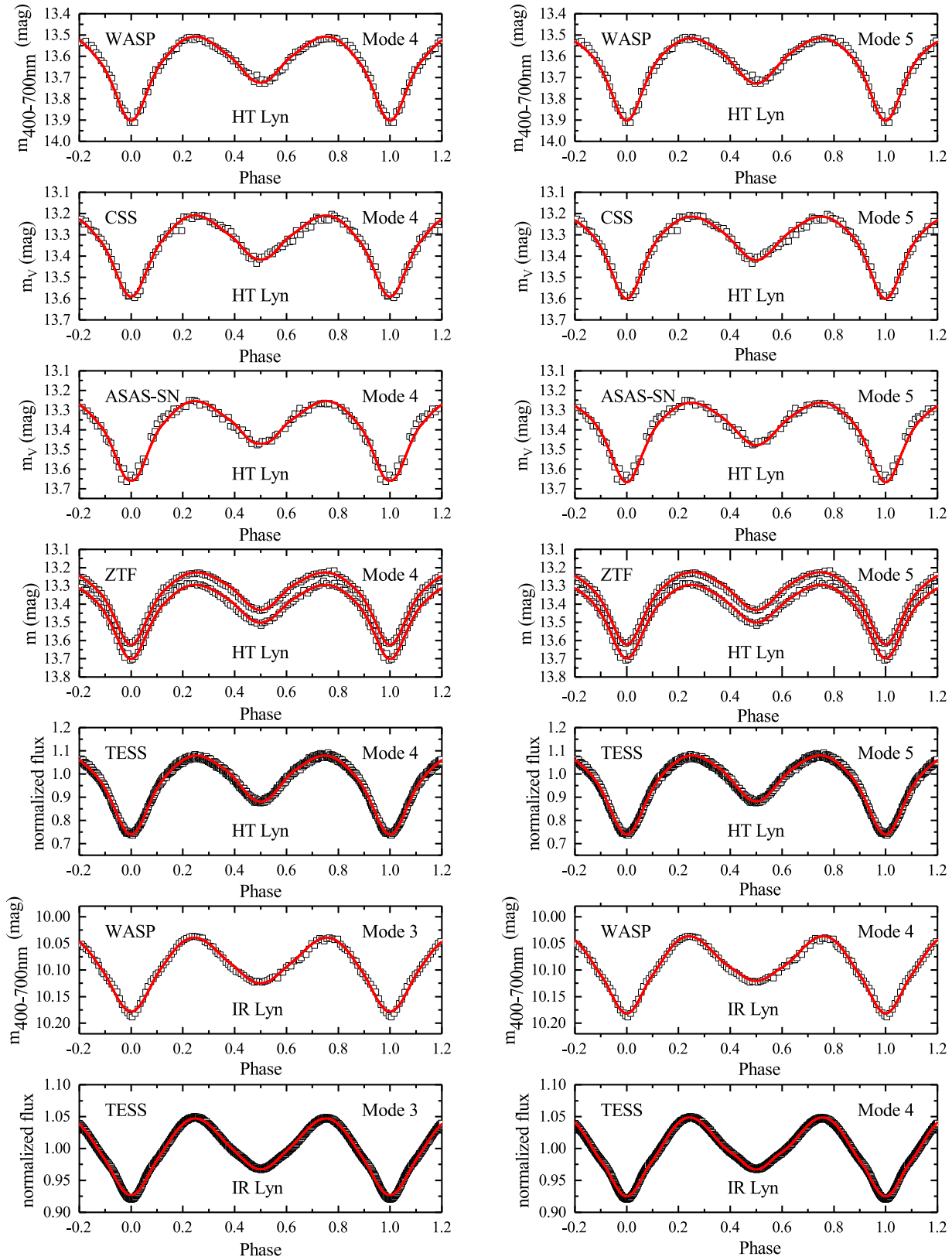

Figure 5. Observed light curves (open squares) for HT Lyn and IR Lyn obtained from several surveys and theoretical light curves (solid lines) calculated from the photometric solutions with different models listed in Tables 7 and 8.

Table 7
Photometric Solutions for the Light Curves from WASP, CSS, ASAS-SN and ZTF

Target Name	HT Lyn								IR Lyn	
Survey	WASP		CSS		ASAS-SN		ZTF		WASP	
Model	mode4(SD1)	mode5(SD2)	mode4(SD1)	mode5(SD2)	mode4(SD1)	mode5(SD2)	mode4(SD1)	mode5(SD2)	mode3(C)	mode4(SD1)
i(degree)	72.54(1.15)	69.26(0.30)	73.51(1.18)	68.70(0.40)	76.52(2.03)	69.55(0.52)	71.61(0.48)	69.87(0.22)	54.04(0.28)	58.10(0.61)
g_1, g_2	1.00,0.32	1.00,0.32	1.00,0.32	1.00,0.32	1.00,0.32	1.00,0.32	1.00,0.32	1.00,0.32	0.32,0.32	0.32,0.32
A_1, A_2	1.00,0.50	1.00,0.50	1.00,0.50	1.00,0.50	1.00,0.50	1.00,0.50	1.00,0.50	1.00,0.50	0.50,0.50	0.50,0.50
$\Omega_{\rm in}$	2.656	2.572	2.611	2.597	2.612	2.608	2.555	2.546	2.294	2.392
Ω_1	2.656	2.623(15)	2.611	2.643(15)	2.612	2.642(20)	2.603	2.556(17)	2.291(2)	2.392
Ω_2	3.020(67)	2.572	3.076(94)	2.597	3.091(109)	2.608	2.655(22)	2.546	2.291(2)	2.729(34)
T_1(K)	7729	7768	7729	7768	7729	7768	7729	7768	6762	6720
T_2(K)	5290(83)	5559(72)	5210(119)	5370(90)	5277(126)	5434(109)	5127(27)	5165(26)	4850(76)	4070(203)
$q=\frac{M_2}{M_1}$	0.389(32)	0.349(17)	0.368(34)	0.361(12)	0.368(28)	0.366(35)	0.341(9)	0.337(7)	0.225(1)	0.267(13)
$\frac{L_1}{L_1+L_2}$	0.958(10)	0.916(6)	0.962(13)	0.925(7)	0.965(10)	0.920(9)	0.951(5)	0.928(4)	0.953(5)	0.991(6)
r_1 (pole)	0.4349(73)	0.4343(27)	0.4396(81)	0.4326(28)	0.4395(67)	0.4337(36)	0.4458(20)	0.4447(21)	0.4788(23)	0.4651(36)
r_1 (side)	0.4644(79)	0.4626(35)	0.4700(94)	0.4607(37)	0.4699(77)	0.4622(47)	0.4775(24)	0.4760(27)	0.5190(37)	0.5014(45)
r_1 (back)	0.4911(83)	0.4856(43)	0.4963(101)	0.4842(45)	0.4962(85)	0.4864(58)	0.5034(23)	0.5012(29)	0.5425(59)	0.5259(42)
r_2 (pole)	0.2239(126)	0.2723(54)	0.2065(106)	0.2748(33)	0.2050(126)	0.2758(57)	0.2514(75)	0.2696(15)	0.2411(12)	0.1934(92)
r_2 (side)	0.2286(137)	0.2837(66)	0.2100(113)	0.2863(41)	0.2084(135)	0.2874(62)	0.2597(87)	0.2809(16)	0.2509(15)	0.1968(100)
r_2 (back)	0.2390(164)	0.3164(68)	0.2178(131)	0.3190(48)	0.2159(157)	0.3201(67)	0.2816(128)	0.3136(16)	0.2839(28)	0.2053(123)
$f=\frac{\Omega_{\rm in}-\Omega}{\Omega_{\rm in}-\Omega_{\rm out}}$	…	…	…	…	…	…	…	…	2.0(1.4)%	…
χ^2	3.507	2.993	0.251	0.223	1.264	1.200	6.132	5.973	9.517	6.827

Table 8
Photometric Solutions for the Light Curves from TESS

Target Name	HT Lyn		IR Lyn	
Model	Mode4 (SD1)	Mode5 (SD2)	Mode3 (C)	Mode4 (SD1)
i(degree)	72.19(26)	70.31(12)	51.47(14)	56.83(8)
g_1, g_2	1.00,0.32	1.00,0.32	0.32,0.32	0.32,0.32
A_1, A_2	1.00,0.50	1.00,0.50	0.50,0.50	0.50,0.50
$\Omega_{\rm in}$	2.560	2.602	2.308	2.376
Ω_1	2.560	2.618(11)	2.306(2)	2.376
Ω_2	2.641(16)	2.602	2.306(2)	2.755(8)
T_1(K)	7729	7768	6762	6720
T_2(K)	5229(15)	5232(15)	4892(13)	4664(22)
$q=\frac{M_2}{M_1}$	0.343(5)	0.363(4)	0.231(1)	0.260(2)
$\frac{L_1}{L_1+L_2}$	0.924(3)	0.908(2)	0.932(1)	0.969(1)
r_1 (pole)	0.4452(11)	0.4375(13)	0.4766(13)	0.4672(6)
r_1 (side)	0.4768(13)	0.4672(16)	0.5161(17)	0.5041(8)
r_1 (back)	0.5027(12)	0.4924(17)	0.5397(18)	0.5283(7)
r_2 (pole)	0.2556(50)	0.2753(9)	0.2428(47)	0.1854(18)
r_2 (side)	0.2644(58)	0.2869(9)	0.2526(56)	0.1884(19)
r_2 (back)	0.2879(87)	0.3196(9)	0.2853(102)	0.1956(23)
$f=\frac{\Omega_{\rm in}-\Omega}{\Omega_{\rm in}-\Omega_{\rm out}}$	...	...	1.5(1.5)%	...
$\sum(O-C)^2$	0.0294	0.0285	0.0089	0.0029

5. Absolute Parameters and Status of Evolution

Owing to the absence of the radial-velocity curves, we calculated the absolute parameters of HT Lyn and IR Lyn using two different methods. One is the Gaia-distance-based scheme proposed by Kjurkchieva et al. (2019a) and developed by Liu et al. (2020) and Li et al. (2021). It has been widely applied for many eclipse binaries (Kjurkchieva et al. 2019a, 2019b, 2020; Li et al. 2019). Also, it was recently proved to be efficient to determine the absolute parameters of eclipse binaries (Li et al. 2021). The other is based on empirical relations to estimate the absolute parameters. However, a reliable empirical relation for NCBs is yet missed so far. Thus, we performed a careful search for the NCBs with reliable physical parameters. A catalog of 48 individually studied samples has been collected and compiled in Table 9. Among them, 25 samples were collected by Yakut & Eggleton (2005). By analyzing all possible correlations among the physical parameters, we found that the semimajor axis and orbital period for NCBs follow an excellent linear relation in the double logarithmic coordinates (see Figure 6). With the least-square method, we derived the following linear relation

$$\log a = 0.914(42)\log P + 0.800(12). \quad (6)$$

The relation would be useful for quick estimating or checking the physical parameters of the numerous NCBs photometrically observed by various surveys. With Equation (6), we can estimate the semimajor axis of HT Lyn and IR Lyn according to their orbital periods. The other physical parameters of them

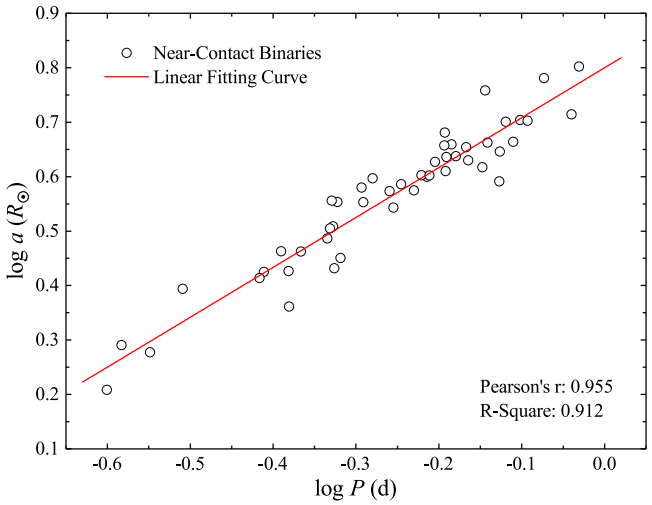

Figure 6. Relation between the orbital period and semimajor axis of NCBs.

are then calculated by combining the semimajor axis with Kepler's third law and the photometric solutions derived from our ground-based observations. As can be seen from Table 10, the absolute parameters estimated by the empirical relation are well consistent with those determined from the Gaia-distance-based scheme, implying that they should be reliable. Finally, by assigning the reciprocals of the errors' square ($1/\sigma^2$) as their weights, the weighted average values of the two set parameters are calculated and adopted in the following analysis.

According to the absolute physical parameters, we located two components of HT Lyn and IR Lyn in the $\log T_{\rm eff}-\log L/L_\odot$, $\log M/M_\odot-\log L/L_\odot$ and $\log M/M_\odot-\log R/R_\odot$ diagrams (Figure 7) to analyze their evolutionary states. For comparison, the NCBs compiled in Table 9 are also added to these diagrams. In Figure 7, the Zero-Age Main Sequence (ZAMS) and Terminal-Age Main Sequence (TAMS) lines are calculated by using the PARSEC models[15] (Bressan et al. 2012). Similar to other NCBs, the primary components of HT Lyn and IR Lyn are located on the main-sequence belt. The secondary components significantly deviate from the main sequence belt and show the over-size and over-luminosity features relative to the single star with the same mass. They have radii about 2–4 times larger than those expected for the corresponding ZAMS masses. Both Lucy (1968) and Moses (1976) suggested the over-size and over-luminous phenomena for the less massive components are caused by the energy transfer from the more massive component to the less massive one. However, it seems physically hard to inflate a ZAMS star to such size purely by the energy transfer from its more massive companion (Stępień 2004). So, the less massive components should be more evolved with hydrogen depleted in their centers.

[15] http://stev.oapd.inaf.it/cgi-bin/cmd

Table 9
Physical Parameters of 48 Individually Studied NCBs

Name	Period	a	M_1	M_2	R_1	R_2	L_1	L_2	T_1	T_2	$\log J_o$	References
FS Aur	0.2508	1.616	0.590	0.310	0.673	0.477	0.115	0.028	4100	3425	51.171	1
VZ Psc	0.2613	1.952	0.810	0.650	0.780	0.700	0.224	0.126	4500	4110	51.566	2
V361 Lyr	0.3096	2.479	1.260	0.870	1.020	0.720	1.479	0.204	6200	4500	51.854	3
CN And	0.4628	3.066	1.299	0.505	1.425	0.916	3.236	0.933	6500	5922	51.713	4
FT Lup	0.4701	3.228	1.430	0.610	1.430	0.940	3.802	0.186	6700	3916	51.821	5
CX Aqr	0.5560	3.492	1.202	0.645	1.318	1.148	2.884	0.831	6457	5248	51.809	6
RT Scl	0.5116	3.575	1.630	0.710	1.590	1.010	5.600	0.360	7000	4820	51.937	7
V1010 Oph	0.6614	4.340	1.732	0.773	1.960	1.322	11.220	1.175	7500	5200	52.027	8, 9
GO Cyg	0.7178	5.732	3.200	1.700	2.630	1.470	85.114	2.754	11200	6200	52.551	10, 11
TT Her	0.9121	5.180	1.560	0.680	2.300	1.490	13.000	0.960	7240	4690	51.989	12
RU Umi	0.5249	3.955	2.290	0.720	1.780	1.110	7.990	0.580	7300	4802	52.058	13
RZ Dra	0.5500	3.746	1.630	0.700	1.650	1.150	9.720	0.740	7940	5006	51.942	14
V836 Cyg	0.6534	4.561	2.200	0.780	1.940	1.340	31.000	1.400	9790	5462	52.108	15, 16
DI Peg	0.7118	4.143	1.184	0.698	1.412	1.374	3.820	0.750	6800	4586	51.870	17
RV Crv	0.7473	4.425	1.640	0.440	2.160	1.200	8.400	1.200	6600	5070	51.803	18
FO Vir	0.7756	4.615	1.900	0.290	2.489	1.060	15.849	0.479	7400	4700	51.684	19
YY Cet	0.7905	5.060	1.840	0.940	2.090	1.630	12.700	2.000	7500	5314	52.149	20
W Crv	0.3881	2.663	1.000	0.680	1.010	0.920	0.970	0.440	5700	4900	51.714	21, 22, 23
BX And	0.6101	3.980	1.520	0.750	1.780	1.300	6.166	0.631	6800	4500	51.960	24
DO Cas	0.6847	4.266	1.690	0.530	2.100	1.200	26.303	0.692	9070	4828	51.875	25
BL Eri	0.4162	2.299	0.610	0.330	0.990	0.730	1.148	0.490	6000	5670	51.279	26
EE Aqr	0.5090	3.800	2.140	0.700	1.790	1.060	7.800	0.330	7227	4233	52.020	27, 28
RS Ind	0.6241	4.238	2.000	0.620	2.000	1.180	9.630	0.590	7200	4659	51.979	28
AG Vir	0.6427	4.077	1.670	0.530	1.970	1.140	10.471	1.862	7400	6300	51.862	29
SW Lyn	0.6441	4.325	1.716	0.899	1.762	1.219	6.457	0.617	6700	4480	52.079	30
CX Vir	0.7461	3.901	1.070	0.360	1.850	1.120	5.650	0.490	6500	4513	51.585	31
BS Vul	0.4760	3.578	2.030	0.680	1.710	1.030	5.400	0.410	6810	4615	51.982	32, 33
GSC2750-0054	0.4719	2.704	0.720	0.470	0.810	0.620	0.270	0.100	4650	4152	51.489	34
V432 Per	0.3833	2.593	1.220	0.370	1.250	0.710	1.600	0.260	5800	4903	51.542	35
BL And	0.7224	4.600	1.800	0.700	2.130	1.350	12.860	0.920	7500	4830	52.014	36
GW Tau	0.6413	4.798	2.750	0.850	2.350	1.380	29.000	1.700	8750	5617	52.212	36
GSC3658-0076	0.7598	5.021	2.180	0.760	2.400	0.980	28.630	0.870	8630	5630	52.117	37
LL Com	0.4069	2.903	1.550	0.430	1.340	0.790	4.100	0.600	7100	5707	51.688	38
UU Lyn	0.4685	3.596	2.100	0.740	1.690	1.020	5.160	0.500	6700	4804	52.024	39
AD Cnc	0.2827	1.894	0.900	0.240	0.960	0.550	0.370	0.190	5164	4595	51.226	40
TW CrB	0.5889	3.757	1.190	0.860	1.440	1.280	2.840	1.970	6250	6050	51.923	41
GR Tau	0.4299	2.901	1.450	0.320	1.490	0.710	6.380	0.060	7500	3434	51.555	42
V473 Cas	0.4155	2.671	1.000	0.480	1.190	0.830	5.700	0.230	5830	4418	51.591	43
II Per	0.4799	2.823	0.950	0.360	1.310	0.840	6.860	0.250	5740	4464	51.482	43
BF Vir	0.6406	4.542	2.040	1.020	1.850	1.440	22.250	1.230	9750	5560	52.185	44
AX Dra	0.5682	3.856	1.460	0.920	1.520	1.370	4.440	1.010	6850	4951	52.014	45
ZZ Aur	0.6012	4.004	1.620	0.760	1.730	1.260	9.780	0.860	7800	4978	51.984	46
AS Ser	0.4662	3.199	1.500	0.520	1.520	0.930	4.970	0.340	7000	4642	51.773	47
KW Per	0.9313	6.346	2.780	1.170	2.120	1.950	30.580	2.560	9340	5213	52.396	48
NP Aqr	0.8070	5.043	1.650	0.990	2.130	1.670	10.000	0.832	7050	4250	52.135	49
KR Cyg	0.8452	6.041	2.876	1.261	2.594	1.804	56.234	2.844	9810	5580	52.423	50, 51
IR Cas	0.6807	4.508	1.430	1.220	1.770	1.510	5.850	2.630	6750	5992	52.138	52
DI Hya	0.6147	4.000	1.600	0.670	1.613	1.195	6.669	0.551	7300	4548	51.934	53

References. (1) Austin (2006); (2) Hrivnak et al. (1995); (3) Hilditch et al. (1997); (4) Van Hamme et al. (2001); (5) Lipari & Sistero (1986); (6) Hilditch et al. (1988); (7) Hilditch & King (1986); (8) Shaw et al. (1990); (9) Corcoran et al. (1991); (10) Rovithis et al. (1990); (11) Ovenden (1954); (12) Milano et al. (1989); (13) Zhu et al. (2006); (14) Erdem et al. (2011); (15) Yakut et al. (2005); (16) Duerbeck & Schumann (1982); (17) Lu (1992); (18) McFarlane et al. (1986a); (19) Mochnacki et al. (1986); (20) McFarlane et al. (1986b); (21) Rucinski & Lu (2000); (22) Odell (1996); (23) Yakut & Eggleton (2005); (24) Bell et al. (1990b); (25) Oh & Ahn (1992); (26) Yamasaki et al. (1988); (27) Covino et al. (1990); (28) Hilditch & King (1988a); (29) Bell et al. (1990a); (30) Kreiner et al. (2003); (31) Hilditch & King (1988b); (32) Nelson (2021); (33) L. Y. Zhu et al. (2012); (34) Elkhateeb & Nouh (2016); (35) Odell et al. (2009); (36) Zhu & Qian (2006); (37) Zhu et al. (2005); (38) Hu et al. (2019); (39) Zhu et al. (2007); (40) Yang & Liu (2002); (41) Zhang & Zhang (2003); (42) Gu et al. (2004); (43) Zhu et al. (2009); (44) L. Zhu et al. (2012); (45) Kim et al. (2004); (46) Oh et al. (2006); (47) Zhu et al. (2008); (48) Gális et al. (2001); (49) İbanoğlu et al. (2010); (50) Sipahi et al. (2013); (51) Sipahi (2005); (52) Li et al. (2014); (53) Liao et al. (2017).

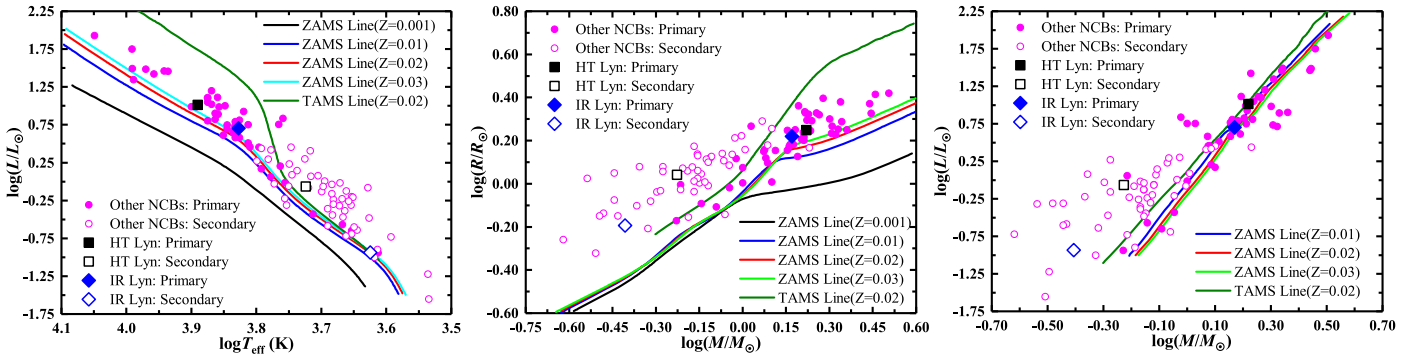

Figure 7. Temperature–Luminosity (left), Mass–Radius (middle), and Mass–Luminosity (right) diagrams.

Table 10
Absolute Physical Parameters of HT Lyn and IR Lyn Calculated from Two Different Methods and Their Weighted Means

Target	Method	$a(R_\odot)$	$M_1(M_\odot)$	$M_2(M_\odot)$	$R_1(R_\odot)$	$R_2(R_\odot)$	$L_1(L_\odot)$	$L_2(L_\odot)$
HT Lyn	GD	3.841(0.297)	1.758(0.408)	0.627(0.153)	1.804(0.145)	1.122(0.090)	10.691(1.831)	0.893(0.156)
	ER	3.739(0.193)	1.620(0.256)	0.579(0.098)	1.756(0.097)	1.092(0.060)	10.126(1.215)	0.846(0.105)
	WM	3.769(0.162)	1.659(0.217)	0.593(0.083)	1.771(0.081)	1.101(0.050)	10.299(1.012)	0.861(0.087)
IR Lyn	GD	3.244(0.195)	1.373(0.247)	0.364(0.079)	1.614(0.104)	0.622(0.045)	4.793(0.902)	0.110(0.029)
	ER	3.426(0.191)	1.618(0.283)	0.429(0.091)	1.705(0.102)	0.657(0.045)	5.347(0.960)	0.123(0.032)
	WM	3.337(0.136)	1.479(0.186)	0.392(0.060)	1.660(0.073)	0.640(0.032)	5.053(0.657)	0.116(0.021)

Note. GD and ER denote the Gaia-Distance-based and the Empirical-Relation-based methods, respectively. WM denotes the weighted means of two sets parameters calculated from the two methods. The standard error in parentheses are calculated according to the error propagation rule.

Because of the marginal contact configuration, the NCBs might be located just in the critical and rare stage predicted by the TRO theory (Flannery 1976; Lucy 1976; Robertson & Eggleton 1977). According to this theory, the close detached binaries have to undergo a few dozens of TRO cycles around the marginal contact status to achieve the over-contact and thermal-equilibrium one. Usually, if an NCB is in the semi-detached or contact stage, it should be undergoing the mass transfer between two components (Qian 2002), resulting in an orbital-period increase or decrease, just like V361 Lyr (Hilditch et al. 1997), V473 Cas and II Per (Zhu et al. 2009), LL Com (Hu et al. 2019), etc. However, both HT Lyn and IR Lyn did not show any significant orbital-period variations at the current stage. Perhaps, HT Lyn and IR Lyn are evolving just from the detached status to the semi-detached one or from the semi-detached status to the detached one. Moreover, the mass transfer is not yet triggered (Zhu et al. 2005) or has just been stopped. From this perspective, HT Lyn and IR Lyn should be two especial sources for testing the TRO theory, and the follow-up monitors should be performed to trace their further evolutions.

6. Conclusion

In this paper, we performed a detailed photometric and orbital period investigation for two NCBs: HT Lyn and IR Lyn. Also, we compiled a catalog of NCBs and derived an empirical relation between the semimajor axis and orbital period. Finally, we discussed their evolutional status. From these investigations, we could draw out the following conclusions: (1) the orbital periods of HT Lyn and IR Lyn were stable for the last two decades; (2) HT Lyn and IR Lyn are two semi-detached NCBs with the secondary and primary filling the Roche lobe; (3) the absolute physical parameters of HT Lyn and IR Lyn were well determined; (4) the primary components of NCBs are, in general, evolving in the main-sequence stage, while their secondary stars are oversize and over-luminosity with respect to the main-sequence star with the same masses.

Acknowledgments

We are grateful to the anonymous referee for constructive comments and suggestions, which have proved to be very helpful for improving the manuscript. This work is supported by the Joint Research Funds in Astronomy (U1931115, U2031114 and U1731110) under cooperative agreement between the National Natural Science Foundation of China and the Chinese Academy of Sciences. We acknowledge the support of the staff of the Xinglong 60 cm telescope. This work was partially supported by the Open Project Program of the

Key Laboratory of Optical Astronomy, National Astronomical Observatories, Chinese Academy of Sciences.

We acknowledge the following surveys for their valuable spectroscopic or photometric data: (1) Guo Shou Jing Telescope (the Large Sky Area Multi-Object Fiber Spectroscopic Telescope, LAMOST) ,which is a National Major Scientific Project built by the Chinese Academy of Sciences. Funding for the project has been provided by the National Development and Reform Commission. LAMOST is operated and managed by the National Astronomical Observatories, Chinese Academy of Sciences; (2) the European Space Agency (ESA) mission Gaia[16] (Gaia Collaboration et al. 2016, 2018), processed by the Gaia Data Processing and Analysis Consortium (DPAC[17]). Funding for the DPAC has been provided by national institutions, in particular the institutions participating in the Gaia Multilateral Agreement; (3) the Northern Sky Variability Survey (NSVS, Woźniak et al. 2004), whose data were collected by the first generation Robotic Optical Transient Search Experiment; (4) the Wide Angle Search for Planets (WASP, Butters et al. 2010), where the data we used is from the DR1 of the WASP data as provided by the WASP consortium, and the computing and storage facilities at the CERIT Scientific Cloud, reg. no. CZ.1.05/3.2.00/08.0144 which is operated by Masaryk University, Czech Republic; (5) the All-Sky Automated Survey for SuperNovae (ASAS-SN, Shappee et al. 2014; Jayasinghe et al. 2019), which consists of two telescopes on a common mount which is hosted by Las Cumbres Observatory Global Telescope Network in the Faulkes Telescope North enclosure on Mount Haleakala, Hawaii; (6) the Catalina Real-Time Transient Survey (CRTS, Drake et al. 2009), a synoptic astronomical exploration that covers thirty three thousand square degrees of the sky in order discover rare and interesting transient phenomena. The survey utilizes data taken by the three dedicated telescopes of the highly successful Catalina Sky Survey (CSS) NEO project. CRTS detects and openly publishes all transients within minutes of observation so that all astronomers may follow ongoing events; (7) the Zwicky Transient Facility (ZTF, Bellm et al. 2019), which is a fully automated, wide-field survey aimed at a systematic exploration of the optical transient sky; (8) the Transiting Exoplanet Survey Satellite (TESS, Ricker et al. 2015) mission. Funding for the TESS mission is provided by the NASA's Science Mission Directorate; (9) the Kamogata/Kiso/Kyoto Wide-field Survey (KWS, Maehara 2014), which has a field-of-view of $5^\circ \times 7.^\circ 5$ and could cover a survey area of about $100^\circ \times 120^\circ$ per night (8 hr); (10) the Two Micron All Sky Survey (Skrutskie et al. 2006), a joint project of the University of Massachusetts and the Infrared Processing and Analysis Center/California Institute of Technology, funded by the National Aeronautics and Space Administration and the National Science Foundation; and (11) The Sloan Digital Sky Survey (Alam et al. 2015; Blanton et al. 2017), funding it has been provided by the Alfred P. Sloan Foundation, the U.S. Department of Energy Office of Science, and the Participating Institutions.

[16] https://www.cosmos.esa.int/gaia
[17] https://www.cosmos.esa.int/web/gaia/dpac/consortium

Appendix
Supplementary Materials

The complete data for Tables 2 and 3 are presented as two supplementary files: mst1-mrt.txt and mst2-mrt.txt, respectively.

References

Alam, S., Albareti, F. D., Allende Prieto, C., et al. 2015, ApJS, 219, 12
Andrae, R., Fouesneau, M., Creevey, O., et al. 2018, A&A, 616, A8
Austin, S. J. 2006, BAAS, 38, 1218
Bell, S. A., Rainger, P. P., & Hilditch, R. W. 1990a, MNRAS, 247, 632
Bell, S. A., Rainger, P. P., Hill, G., & Hilditch, R. W. 1990b, MNRAS, 244, 328
Bellm, E. C., Kulkarni, S. R., Graham, M. J., et al. 2019, PASP, 131, 018002
Blanton, M. R., Bershady, M. A., Abolfathi, B., et al. 2017, AJ, 154, 28
Borkovits, T., Rappaport, S., Hajdu, T., & Sztakovics, J. 2015, MNRAS, 448, 946
Bressan, A., Marigo, P., Girardi, L., et al. 2012, MNRAS, 427, 127
Butters, O. W., West, R. G., Anderson, D. R., et al. 2010, A&A, 520, L10
Corcoran, M. F., Siah, M. J., & Guinan, E. F. 1991, AJ, 101, 1828
Covey, K. R., Ivezić, Ž., Schlegel, D., et al. 2007, AJ, 134, 2398
Covino, E., Barone, F., Milano, L., Russo, G., & Starna, M. J. 1990, MNRAS, 246, 472
Drake, A. J., Djorgovski, S. G., Mahabal, A., et al. 2009, ApJ, 696, 870
Duerbeck, H. W., & Schumann, J. D. 1982, JAA, 3, 233
Elkhateeb, M. M., & Nouh, M. I. 2016, NewA, 49, 22
Erdem, A., Zola, S., & Winiarski, M. 2011, NewA, 16, 6
Flannery, B. P. 1976, ApJ, 205, 217
Gaia Collaboration, Brown, A. G. A., Vallenari, A., et al. 2018, A&A, 616, A1
Gaia Collaboration, Prusti, T., de Bruijne, J. H. J., et al. 2016, A&A, 595, A1
Gális, R., Hric, L., & Niarchos, P. 2001, A&A, 373, 950
Gu, S.-h., Chen, P.-s., Choy, Y.-k., et al. 2004, A&A, 423, 607
Hilditch, R. W., Collier Cameron, A., Hill, G., Bell, S. A., & Harries, T. J. 1997, MNRAS, 291, 749
Hilditch, R. W., & King, D. J. 1986, MNRAS, 223, 581
Hilditch, R. W., & King, D. J. 1988a, MNRAS, 232, 147
Hilditch, R. W., & King, D. J. 1988b, MNRAS, 231, 397
Hilditch, R. W., King, D. J., & McFarlane, T. M. 1988, MNRAS, 231, 341
Hrivnak, B. J., Guinan, E. F., & Lu, W. 1995, ApJ, 455, 300
Hu, K., Chen, K., Xiang, F.-Y., Yu, Y.-X., & Zhao, E.-G. 2019, AJ, 158, 104
Huang, C. X., Vanderburg, A., Pál, A., et al. 2020, RNAAS, 4, 204
İbanoğlu, C., Çakırlı, Ö., & Dervişoğlu, A. 2010, NewA, 15, 373
Jayasinghe, T., Stanek, K. Z., Kochanek, C. S., et al. 2019, MNRAS, 486, 1907
Kaluzny, J. 1985, AcA, 35, 327
Khruslov, A. V. 2013, PZP, 13, 16
Kim, H. -I., Lee, J. W., Kim, C. -H., et al. 2004, PASP, 116, 931
Kjurkchieva, D., & Vasileva, D. 2015, PASA, 32, e023
Kjurkchieva, D. P., Popov, V. A., Eneva, Y., & Petrov, N. I. 2019a, RAA, 19, 014
Kjurkchieva, D. P., Popov, V. A., & Petrov, N. I. 2019b, AJ, 158, 186
Kjurkchieva, D. P., Popov, V. A., & Petrov, N. I. 2020, NewA, 77, 101352
Kreiner, J. M., Rucinski, S. M., Zola, S., et al. 2003, A&A, 412, 465
Kwee, K. K., & van Woerden, H. 1956, BAN, 12, 327
Li, K., Hu, S. M., Guo, D. F., et al. 2014, AJ, 148, 96
Li, K., Kim, C. -H., Xia, Q. -Q., et al. 2020, AJ, 159, 189
Li, K., Xia, Q. -Q., Kim, C. -H., et al. 2021, AJ, 162, 13
Li, K., Xia, Q. -Q., Liu, J. -Z., et al. 2019, RAA, 19, 147
Liao, W. P., Qian, S. B., Li, L. J., et al. 2017, PASP, 129, 034201
Lipari, S. L., & Sistero, R. F. 1986, MNRAS, 220, 883
Liu, L., Qian, S., Li, K., et al. 2020, Ap&SS, 365, 71
Lu, W. 1992, AcA, 42, 73

Lucy, L. B. 1967, ZAp, 65, 89
Lucy, L. B. 1968, ApJ, 151, 1123
Lucy, L. B. 1976, ApJ, 205, 208
Luo, A. L., Zhao, Y. -H., Zhao, G., et al. 2015, RAA, 15, 1095
Maehara, H. 2014, Jaxa Research & Development Report, 13, 119
Masci, F. J., Laher, R. R., Rusholme, B., et al. 2019, PASP, 131, 018003
McFarlane, T. M., Hilditch, R. W., & King, D. J. 1986a, MNRAS, 223, 595
McFarlane, T. M., King, D. J., & Hilditch, R. W. 1986b, MNRAS, 218, 159
Milano, L., Barone, F., Mancuso, S., Russo, G., & Vittone, A. A. 1989, A&A, 210, 181
Mochnacki, S. W., Fernie, J. D., Lyons, R., Schmidt, F. H., & Gray, R. O. 1986, AJ, 91, 1221
Moses, A. P. 1976, MNRAS, 176, 161
Nelson, R. H. 2021, NewA, 87, 101598
Odell, A. P. 1996, MNRAS, 282, 373
Odell, A. P., Eaton, J. A., & López-Cruz, O. 2009, MNRAS, 400, 2085
Oh, K. -D., & Ahn, Y. -S. 1992, Ap&SS, 187, 261
Oh, K.-D., Kim, C.-H., Lee, W.-B., Kim, H.-I., & Kang, Y.-W. 2006, MNRAS, 366, 1243
Ovenden, M. W. 1954, MNRAS, 114, 569
Pavlovski, K., Cuypers, J., David, M., et al. 1998, A&A, 331, 639
Pecaut, M. J., & Mamajek, E. E. 2013, ApJS, 208, 9
Qian, S. 2002, MNRAS, 336, 1247
Qian, S. B., & Zhu, L. Y. 2002, ApJ, 568, 1004
Ricker, G. R., Winn, J. N., Vanderspek, R., et al. 2015, JATIS, 1, 014003
Robertson, J. A., & Eggleton, P. P. 1977, MNRAS, 179, 359
Rovithis, P., Rovithis-Livaniou, H., & Niarchos, P. G. 1990, A&AS, 83, 41
Ruciński, S. M. 1969, AcA, 19, 245
Rucinski, S. M., & Lu, W. 2000, MNRAS, 315, 587
Schlafly, E. F., & Finkbeiner, D. P. 2011, ApJ, 737, 103
Shappee, B. J., Prieto, J. L., Grupe, D., et al. 2014, ApJ, 788, 48
Shaw, J. S. 1994, MmSAI, 65, 95
Shaw, J. S., Guinan, E. F., & Garasi, C. J. 1990, BAAS, 22, 1296
Sipahi, E. 2005, IBVS, 5635, 1
Sipahi, E., Çakirli, Ö., & Ibanoglu, C. 2013, RMxAA, 49, 25
Skrutskie, M. F., Cutri, R. M., Stiening, R., et al. 2006, AJ, 131, 1163
Stępień, K. 2004, in Stars as Suns: Activity, Evolution and Planets, ed. A. K. Dupree & A. O. Benz, Vol. 219 (San Francisco, CA: ASP), 967
van Hamme, W. 1993, AJ, 106, 2096
Van Hamme, W., Samec, R. G., Gothard, N. W., et al. 2001, AJ, 122, 3436
Wang, K. 2017, RAA, 17, 112
Wilson, R. E. 1979, ApJ, 234, 1054
Wilson, R. E. 1990, ApJ, 356, 613
Wilson, R. E., & Devinney, E. J. 1971, ApJ, 166, 605
Wilson, R. E., & Van Hamme, W. 2014, ApJ, 780, 151
Woźniak, P. R., Vestrand, W. T., Akerlof, C. W., et al. 2004, AJ, 127, 2436
Yakut, K., & Eggleton, P. P. 2005, ApJ, 629, 1055
Yakut, K., Ulaş, B., Kalomeni, B., & Gülmen, Ö. 2005, MNRAS, 363, 1272
Yamasaki, A., Jugaku, J., & Seki, M. 1988, AJ, 95, 894
Yang, Y. -L., & Liu, Q. -Y. 2002, ChJAA, 2, 369
Zejda, M., Zhang, J., Qian, S., Zhu, L., & Mikulášek, Z. 2016, JPCO, 728, 072022
Zhang, X. B., & Zhang, R. X. 2003, AJ, 125, 1431
Zhu, L., & Qian, S. 2006, MNRAS, 367, 423
Zhu, L., Qian, S. -B., & Li, L. 2012, PASJ, 64, 94
Zhu, L., Qian, S. B., Mikulášek, Z., et al. 2010, AJ, 140, 215
Zhu, L. -Y., Qian, S. -B., Boonrucksar, S., He, J. -J., & Yuan, J. -Z. 2007, ChJAA, 7, 251
Zhu, L. -Y., Qian, S. -B., & Xiang, F. -Y. 2006, PASJ, 58, 361
Zhu, L. Y., Qian, S. B., Xiang, F. Y., & González-Rojas, D. J. 2005, Ap&SS, 299, 329
Zhu, L. Y., Qian, S. B., & Yang, Y. G. 2008, AJ, 136, 337
Zhu, L. Y., Qian, S. B., Zola, S., & Kreiner, J. M. 2009, AJ, 137, 3574
Zhu, L. Y., Zejda, M., Mikulášek, Z., et al. 2012, AJ, 144, 37